Lamellar Bridged Silsesquioxanes: Self-Assembly through a Combination of Hydrogen Bonding and Hydrophobic Interactions

Joël J. E. Moreau,*[a] Luc Vellutini,[a] Michel Wong Chi Man,[a] Catherine Bied,[a] Philippe Dieudonné,[b] Jean-Louis Bantignies,[b] and Jean-Louis Sauvajol[b]

Abstract: The synthesis of four bis(trialkoxysilylated) organic molecules capable of self-assembly—$(EtO)_3Si(CH_2)_3NHCONH-(CH_2)_n-NHCONH(CH_2)_3Si(OEt)_3$ (n = 9–12)—associating urea functional groups and alkylidene chains of variable length is described. These compounds behave as organogelators, forming supramolecular assemblies thanks to the intermolecular hydrogen bonding of urea groups. Whereas fluoride ion-catalysed hydrolysis in ethanol in the presence of a stoichiometric amount of water produced amorphous hybrids, acid-catalysed hydrolysis in an excess of water gave rise to the formation of crystalline lamellar hybrid materials through a self-organisation process. The structural features of these nanostructured organic/inorganic hybrids were analysed by several techniques: attenuated Fourier transformed infrared (ATR-FTIR), solid-state NMR spectroscopy (^{13}C and ^{29}Si), scanning and transmission electron microscopy (SEM and TEM) and powder X-ray diffraction (PXRD). The reaction conditions, the hydrophobic properties of the long alkylidene chains and the hydrogen-bonding properties of the urea groups are determining factors in the formation of these self-assembled nanostructured hybrid silicas.

Keywords: bridged silsesquioxanes · gels · nanomaterials · self-assembly · self-organised hybrids

Introduction

The use of sol–gel processing has proved to be a powerful method for the production of solid hybrid materials.[1,2] Over the last decade, polysilsesquioxanes arising from the sol–gel hydrolysis of polysilylated organic molecules[3–8] have allowed the synthesis of new organic/inorganic hybrids by design. The properties of the resulting hybrid solids can be tuned by the introduction of appropriate organic functionality into the silicate network through covalent linkage. Bridged silsesquioxanes have proven efficient, for example, as enantioselective heterogeneous catalysts,[6] as electrochemically active solids,[7] as extracting solids for lanthanides and actinides,[8] as materials for optics and opto-electronics.[9] These functional hybrid silicates, prepared by hydrolysis of alkoxyorganosilanes in solution, are amorphous solids despite some intermolecular interactions, and organisation between the organic fragments has been suspected on the basis of chemical reactivities.[7,10]

Nanostructuring and control over morphology in hybrid solids are of great interest for the design of polyfunctional materials.[11] Recently, the surfactant-mediated pathway,[12] originally used to produce periodic mesoporous silicas, has been successfully extended to bridged silsesquioxanes.[13] The use of an external surfactant resulted in shape-controlled hybrids[14] and in hybrids with highly ordered hexagonal mesoporous structures.[13,14] In silsesquioxane hybrids, the bridging organic unit itself can be used to direct the structure of the solid network without addition of an external structure-directing agent. Weak interactions between precursor molecules during the hydrolysis–condensation of trialkoxysilanes has been shown to influence the kinetic parameters of the gelation[15] and to modify the texture and morphology of silsesquioxane.[16] Anisotropic organisation due to interactions between rigid aromatic units was interestingly demonstrated by the generation of birefringent silsesquioxane materials.[17] Moreover, mesoporous phenylene-

[a] Prof. Dr. J. J. E. Moreau, Dr. L. Vellutini, Dr. M. Wong Chi Man, Dr. C. Bied
Hétérochimie Moléculaire et Macromoléculaire (UMR-CNRS 5076)
Ecole Nationale Supérieure de Chimie de Montpellier
8, rue de l'école normale
34296 Montpellier cédex 5 (France)
Fax: (+33) 467-147-212
E-mail: jmoreau@cit.enscm.fr

[b] Dr. P. Dieudonné, Dr. J.-L. Bantignies, Dr. J.-L. Sauvajol
Groupe de Dynamique des Phases Condensées (UMR-CNRS 5581)
Université de Montpellier II
Place Eugène Bataillon
34095 Montpellier cédex 5 (France)

 DOI: 10.1002/chem.200401012

bridged silsesquioxanes with ordered hexagonal pore structure and crystalline pore walls have been obtained recently.[18]

We recently developed a new and efficient approach for a controlled synthesis of organically bridged silicas through the design and hydrolysis of trialkoxyorganosilanes that exhibit hydrogen-bonding interactions,[9c,19,20] providing a route to the generation of self-organised hybrid silicas. As demonstrated in the case of silicas,[21] transcription of the chiral properties of the molecular precursor to the hybrid solid was achieved. Under acidic conditions in water, helical hybrids with controlled handedness formed upon hydrolysis of the *R*,*R* or *S*,*S* enantiomers of diurea derivatives of *trans*-(1,2)-diaminocyclohexane.[19a] Long-range ordered hybrids were achieved when hydrogen-bonding interactions were combined with aromatic π–π or hydrophobic interaction.[19b,20] The organic bridging substructure plays an important role in controlling the arrangement of the crystalline lamellar material. In the work in this paper we have studied the contribution of the main organic alkylidene bridging substructure in combination with the urea groups in the self-organisation of these hybrid solids. We report self-organised lamellar bridged silsesquioxanes obtained by the acid-catalysed (HCl) hydrolysis of bis(trialkoxysilylated) organic molecules combining urea functional groups and alkylidene chains of variable length: $(EtO)_3Si(CH_2)_3NHCONH{-}(CH_2)_n{-}NHCONH(CH_2)_3Si(OEt)_3$, with n = 9–12. Whereas sol–gel hydrolysis–condensation produced amorphous materials when catalysed by fluoride ion in ethanol, acid-catalysed hydrolysis allowed the generation of long-range ordered self-organised lamellar bridged silsesquioxanes with variable interlamellar distances depending on the lengths of the organic spacers.

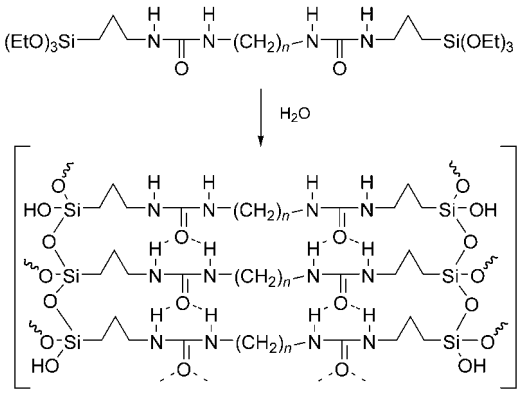

Scheme 1. Synthesis of self-organised lamellar alkylene-bridged silsesquioxanes.

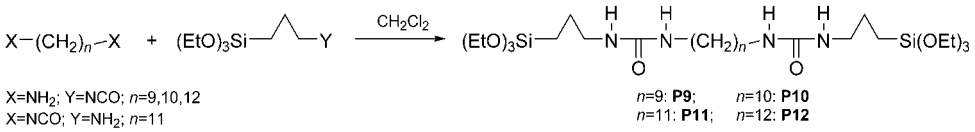

Scheme 2. Synthesis of the precursors **P*x*** (x = 9–12).

Results and Discussion

We have studied how the combination of the self-assembly properties of urea groups[22–24] with the hydrophobic interactions provided by long hydrocarbon chains can direct the hydrolysis–condensation of linear bis-trialkoxysilylalkanes in order to generate self-organised hybrids with tuneable lamellar spacings (Scheme 1).

Synthesis of silyl precursors containing long hydrocarbon chains: The four molecular precursors **P9** to **P12**, containing nine- to twelve-carbon alkylene units, were synthesized by treatment of α,ω-diamino or α,ω-diisocyanato alkanes with 3-(isocyanatopropyl)triethoxysilane or 3-(aminopropyl)triethoxysilane, respectively (Scheme 2).

The reactions between the amino groups and the isocyanates to form ureas were quantitative, and the reaction products were easily purified after elimination of the solvent and washing with dry cold pentane. The pure precursors **P9**–**P12** were isolated as microcrystalline solids in 80–93% yields, and were soluble in CH_2Cl_2, THF or EtOH. As has been observed for related bis(urea)-based molecules[22–24] **P9**–**P12** behave as gelators in $CHCl_3$ or toluene at low concentrations (ca. 10 g L^{-1}). Evidence for the intermolecular association of the urea groups was obtained from the FTIR spectra of the precursors **P9**–**P12** in solution and in the solid state. Diluted $CHCl_3$ solutions of the precursors showed the vibrations characteristic of free urea groups:[25] ν_{N-H} = 3445, $\nu_{C=O}$ (amide I) = 1654 and δ_{N-H} (amide II) = 1538 cm^{-1}. At higher concentrations, as organogels the vibration bands shifted towards lower frequencies: −125 cm^{-1} for ν_{N-H} and −35 cm^{-1} for $\nu_{C=O}$. At the same time, the δ_{N-H} band shifted by +35 cm^{-1} towards higher frequencies. This behaviour is characteristic of strongly associated urea groups between **P9**–**P12** molecules.[25] In the solid state, the observed vibrations for the four microcrystalline precursors appeared at 1623 cm^{-1} ($\nu_{C=O}$) and 1577 cm^{-1} (δ_{N-H}). The Δν value ($\nu_{C=O}-\delta_{N-H}$) of 46 cm^{-1} is indicative of strong association of the urea groups by hydrogen bonds. No significant variation in the hydrogen bond strength as a function of chain length (nine to twelve carbon atoms) was observed, since identical Δν values were measured for **P9**–**P12**. Some differences appeared in the ν_{N-H} region, with the solid-state spectra of **P9**–**P12** exhibiting bands at 3347 and 3319 cm^{-1}, in comparison with the solution spectra (ν_{N-H} = 3445 cm^{-1}) and the gel spectra (ν_{N-H} = 3320 cm^{-1}). These are indicative of two types of N−H bonds, the stronger being centred at low frequency (3319 cm^{-1}) at a value close to the value observed in the organogel. Similar behaviour was observed for all precursor molecules whatever the length of the alkylene chain. Clearly the intermolecular associations by hydrogen bonds are weakly sensitive to the length of the spacer.

Hydrolysis–condensation of P9–P12: The hydrolysis–condensation of the four precursors, to give hybrid networks, was performed under two different sets of reaction conditions: with nucleophilic catalysis, in which case the condensation is the faster reaction, and with acid catalysis, in which hydrolysis is the faster step.

This was first achieved under normal sol–gel conditions by dissolution of the molecular precursor in ethanol and subsequent addition of a stoichiometric amount of water (6 mol equiv) and a catalytic quantity of NH_4F. The viscosity of the reaction mixture increased up to the formation of a transparent gel phase after 24 h. The system was cured for 48 h, and the obtained solid materials **A9**–**A12** were dried overnight at 110 °C (Scheme 3). We then studied different reaction conditions without EtOH solvent, with use of a large excess of water to favour hydrophobic intermolecular interaction between precursor molecules. Hydrolysis–condensation was achieved in the presence of HCl as catalyst (pH 2; to ensure fast hydrolysis of the precursors). Products obtained in this manner were not soluble but partly dissolved upon hydrolysis. Heating of the heterogeneous mixture at 80 °C for 48 h resulted in condensation and afforded the solid materials **L9**–**L12** (Scheme 3) after drying as in the previous case.

The compositions of the hybrid materials **A9**–**A12** and **L9**–**L12** were characterised by elemental analysis and by ^{13}C and ^{29}Si solid-state NMR spectroscopy. The analysis revealed N/Si ratios of 2:1 for all solids, consistent with the structures represented in Scheme 3, indicating that the organic substructure was retained during the hydrolysis–condensation whatever the reaction conditions; this was also confirmed upon examination of the solid-state ^{13}C NMR spectra of all materials. The spectra of **A12** and **L12** are shown in Figure 1 as examples.

The signals at $\delta = 160$, 43, 34, 31, 26 and 11 ppm correspond to the carbonyl and sp^3 carbon atoms of the alkyl chain. The absence of signals at $\delta = 18$ and 58 ppm (ethoxy groups) is indicative of complete hydrolysis of the Si–OEt groups under the reaction conditions. Interestingly, the lines in **L12** appeared narrower than their counterparts in **A12**, which reflects a more homogeneous arrangement and higher mobility of the organic substructure in **L12** than in **A12**. Similar observations were made for the other materials, and were confirmed upon examination of the ^{29}Si NMR spectra (Figure 2).

Broader signals were observed for **A12**, with resonances at $\delta = -58$ [T^2: $CSi(OSi)_2OH$] and -67 ppm [T^3: $CSi(OSi)_3$] corresponding to a degree of condensation of 90 %. The

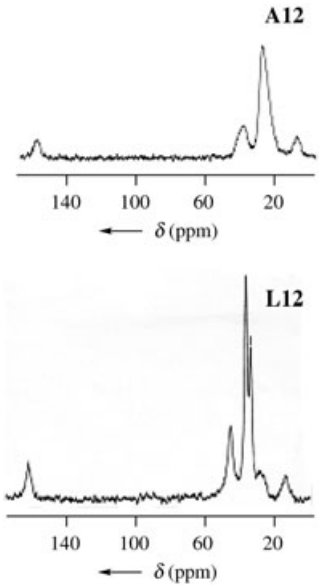

Figure 1. ^{13}C CP-MAS solid-state NMR spectra of hybrid silicas **A12** and **L12**.

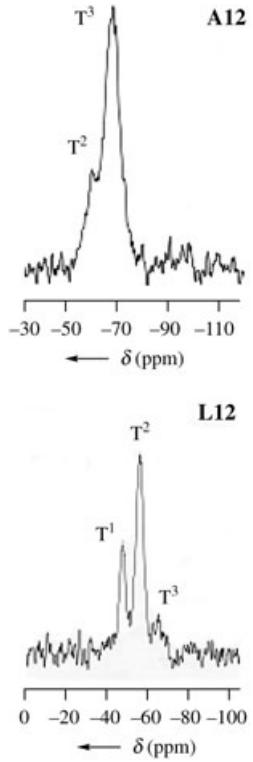

Figure 2. ^{29}Si CP-MAS NMR solid-state spectra of hybrid silicas **A12** and **L12**.

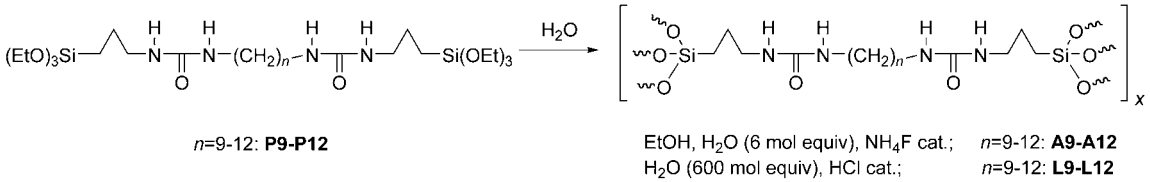

Scheme 3. Synthesis of lamellar (**L9**–**L12**) or amorphous (**A9**–**A12**) bridged silsesquioxanes.

spectra of **L12** revealed sharper signals at $\delta = -49$ [T^1: $CSi(OSi)(OH)_2$], -58 [T^2: $CSi(OSi)_2OH$] and -67 ppm [T^3: $CSi(OSi)_3$] with a degree of condensation of 65%. The much higher degree of condensation, resulting in a more rigid hybrid network in **A12** than in **L12**, is consistent with the previous NMR observations, and is a result of the different reaction conditions. Fluoride ion catalysis gives fast condensation in relation to the hydrolysis rate, and results in a highly condensed and rigid hybrid network. Conversely, rapid hydrolysis and slower condensation occur in the acid-catalysed reaction and this results in a less condensed hybrid network.[4,26]

Structural ordering in hybrids A9–A12 and L9–L12: X-ray analysis of the various hybrids revealed interesting features. The diffraction diagrams of materials **A9–A12** showed broad bands consistent with essentially amorphous structures, as usually observed for related silsesquioxanes.[3,4] Conversely, the X-ray diffraction spectra of materials **L9–L12** showed intense Bragg peaks indicative of medium- to long-range ordered lamellar structures (Figure 3).

A first intense peak (001) at a low q value (0.241, 0.240, 0.229 and 0.215 $Å^{-1}$ for hybrids **L9** to **L12**, respectively) was observed. Peaks of lower intensity at q values of 0.65–0.72 and 0.86–0.96 $Å^{-1}$ could be associated with third (003) and fourth (004) orders of the high intensity peaks (001) at low q values. This corresponds to characteristic distances of 26.3 to 29.2 Å for materials **L9** to **L12**, respectively. Interestingly, these distances are compatible with the lengths of the organic spacers in the precursors containing hydrocarbon chains with nine to twelve carbon atoms. A schematic representation of the structure of the lamellar hybrids is shown in Scheme 4.

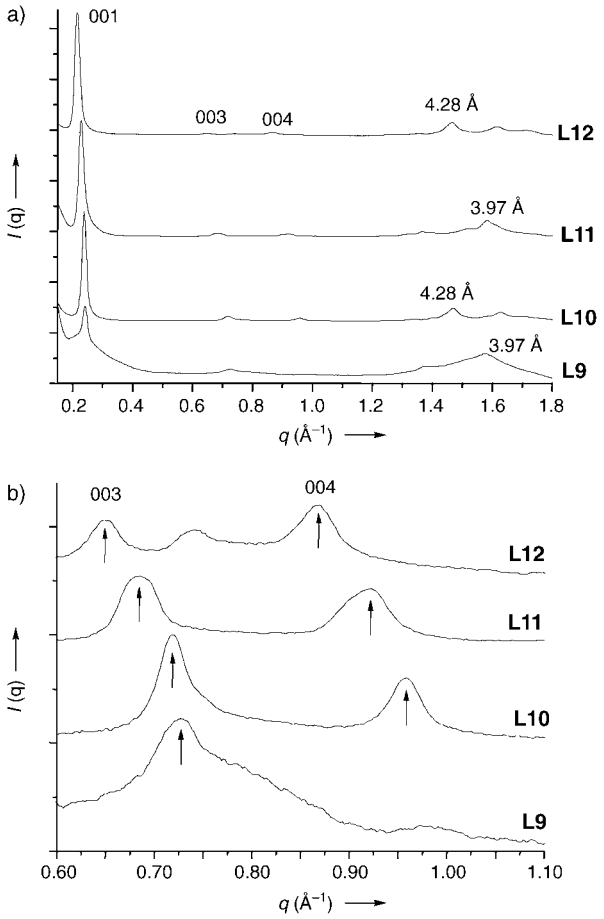

Figure 3. a) X-ray diffraction diagrams of the ordered hybrid silicas **L9–L12**; b) expansion of the region $q = 0.60$–1.10 $Å^{-1}$.

This schematic representation is based on the recent determination of the structures of related materials containing (1,4)-bis(ureido)phenylene-bridged units.[20] It consists of ribbons containing the organic substructures bonded by intermolecular hydrogen bonds of the urea groups. The diffraction peaks at the lowest q values (Figure 3) could describe the distances between silylated ribbons. The other peaks at higher q values (1.45–1.70 $Å^{-1}$) in the diffraction diagrams could be attributed to intermolecular distances along a ribbon controlled by the urea units (4.5 Å) associated through hydrogen bonds or to in-plane ordering.[9c,20]

On going from **L12** to **L9** (Figure 3), the most intense peak shifted towards higher q values, consistently with a decrease in the organic chain length from twelve to nine carbon atoms. At the same time, some broadening of the peaks appeared, indicative of an increase in amorphous character with decreasing chain length. Shorter organic chains containing six to eight carbon atoms have been shown to afford amorphous hybrids whatever the reaction conditions.[27]

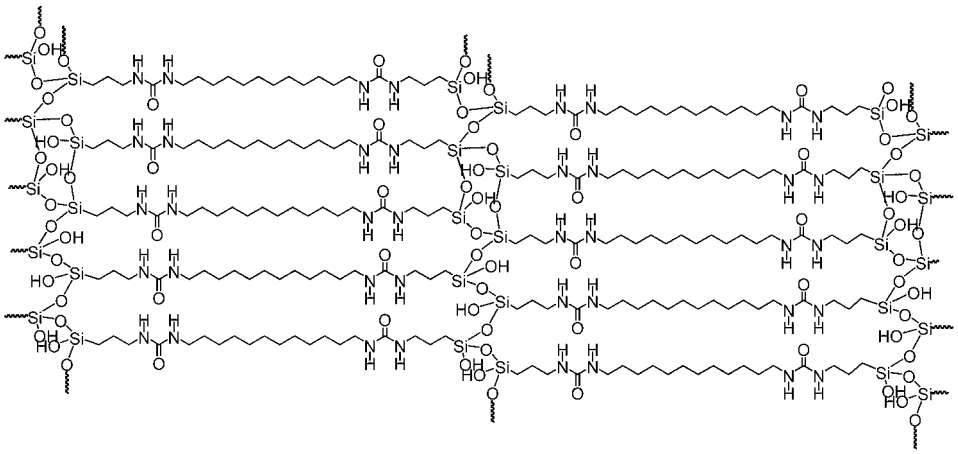

Scheme 4. Schematic representation of the structures of the ordered hybrid silicas **L9–L12**.

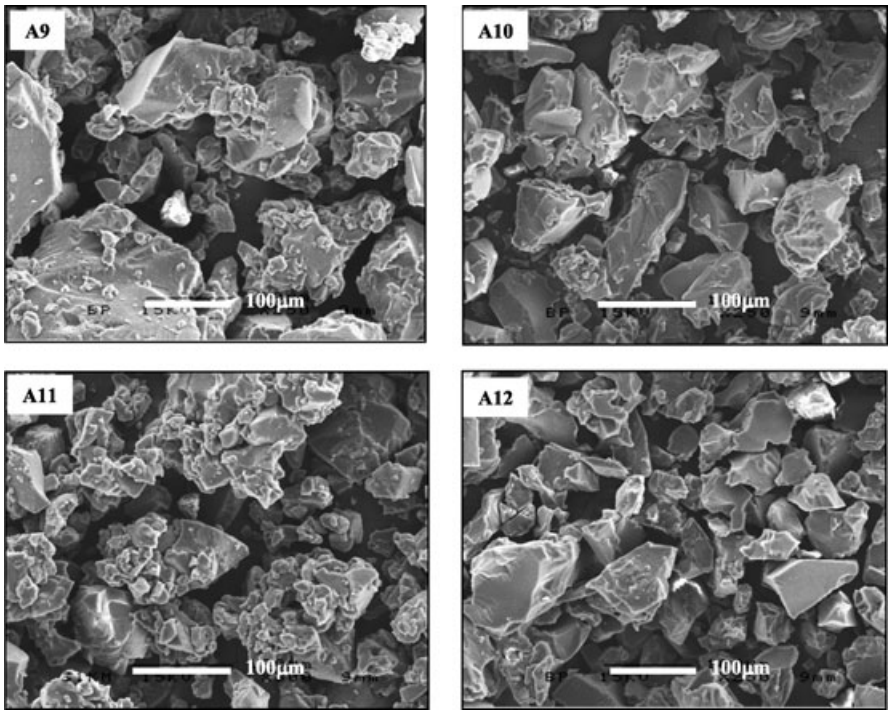

Figure 4. SEM images of amorphous hybrid silicas **A9**–**A12** with granular morphology.

Electron microscopy studies on the various hybrids revealed morphologies consistent with their amorphous or ordered structures. Scanning electron microscopy (SEM) images of materials **A9**–**A12** are presented in Figure 4. These show dense, compact solids with granular morphologies.

Conversely, the hybrids **L9**–**L12** presented homogeneous lamellar morphologies consisting of thin plates 1–3 μm wide, 3–30 μm long and 0.05–0.5 μm thick (Figure 5). These plates look like flexible films, which are still arranged in layers for shorter chain lengths, particularly in **L9**.

Interestingly, the transmission electronic microscopy (TEM) images confirmed the layered structures by showing some well ordered features with lamellar spacings (Figure 6). The interlayer spacings observed in the TEM images are consistent with the lengths of the organic spacers and with the distances calculated from the Bragg peaks at low q values. Additionally, the half-widths at the half-maxima of these peaks allowed correlation lengths of 270–350 Å to be determined, in the same order of magnitude as the plate thickness observed from the TEM images.

The organisation and long-range order in **L9**–**L12** appeared to be dependent on the hydrophobic properties of the alkylene spacers in the organic substructures. The formation of the lamellar hybrid phase was only observed upon hydrolysis–condensation in water, whereas this produced amorphous hybrids when the less hydrophobic ethanol was used. The combination of hydrogen-bond and hydrophobic interactions allowed ordered hybrids to be generated.

Hydrogen-bonding interactions in amorphous and lamellar hybrids: The characteristic IR vibrations of the urea groups are an interesting probe for exploring hydrogen-bonding interactions between organic substructures in the hybrid network and can also provide evidence for preferential orientation and organisation within the materials.

The IR spectra of the amorphous materials **A9** to **A12**, measured at room temperature, are quite similar. The spectrum of **A12** over two wavenumber ranges ($\tilde{\nu}$ = 2800–3500 and 1500–1800 cm^{-1}) is given as an example in Figure 7.

Broad bands are observed at 3374 cm^{-1} (ν_{N-H}), 1645 cm^{-1} ($\nu_{C=O}$) and 1577 cm^{-1} (δ_{N-H}). These wavenumbers are indicative of hydrogen-bonded urea groups, but in agreement with the amorphous character of **A12**, corresponding to a non-homogeneous distribution of hydrogen bonding, which is responsible for the broadening of the bands in the IR spectrum. The lamellar hybrids **L9**–**L12** also gave similar spectra, though with narrower bands than those observed for **A9**–**A12**, centred at 3348 and 3320 cm^{-1} (ν_{N-H}), 1623 cm^{-1} ($\nu_{C=O}$) and 1585 cm^{-1} (δ_{N-H}) (Figure 8).

These vibrations appeared similar to those observed for the precursors in the solid state; however, more strongly hydrogen-bonded urea groups appeared in the lamellar hybrid solid. The value of $\Delta\nu$ (= 38 cm^{-1}) was lower than that in the precursors ($\Delta\nu$ = 46 cm^{-1}). This difference arises from a shift of the δ_{N-H} vibration (1585 versus 1577 cm^{-1}) towards higher frequencies, indicating that N–H deformation is a more sensitive indicator of hydrogen-bonding interactions. The vibration modes also showed temperature dependence, which was studied over the 260 K to 10 K range. The lamellar hybrid **L10** showed $\Delta\nu$ values from 34 cm^{-1} (260 K) to 22 cm^{-1} (10 K) towards lower frequencies, indicating stronger hydrogen-bonding interactions at low temperatures. The same trend, though weaker, was observed in the case of the amorphous solid **A10**, with $\Delta\nu$ values of 72 cm^{-1} (260 K) and 52 cm^{-1} (10 K).

The above results clearly showed that the hydrogen-bonding interactions were playing an important role in controlling the structures of the hybrids. Since hydrogen bonds are directional interactions, it was of interest to explore their possible anisotropic orientation within the solid. This was studied by FTIR by the attenuated total reflection (ATR) technique through examination of the polarisation dependence of the vibration modes. The FTIR-ATR spectra of the amorphous **A12** and lamellar **L12** hybrids are shown in Figure 9. H-polarisation refers to transmission spectra ob-

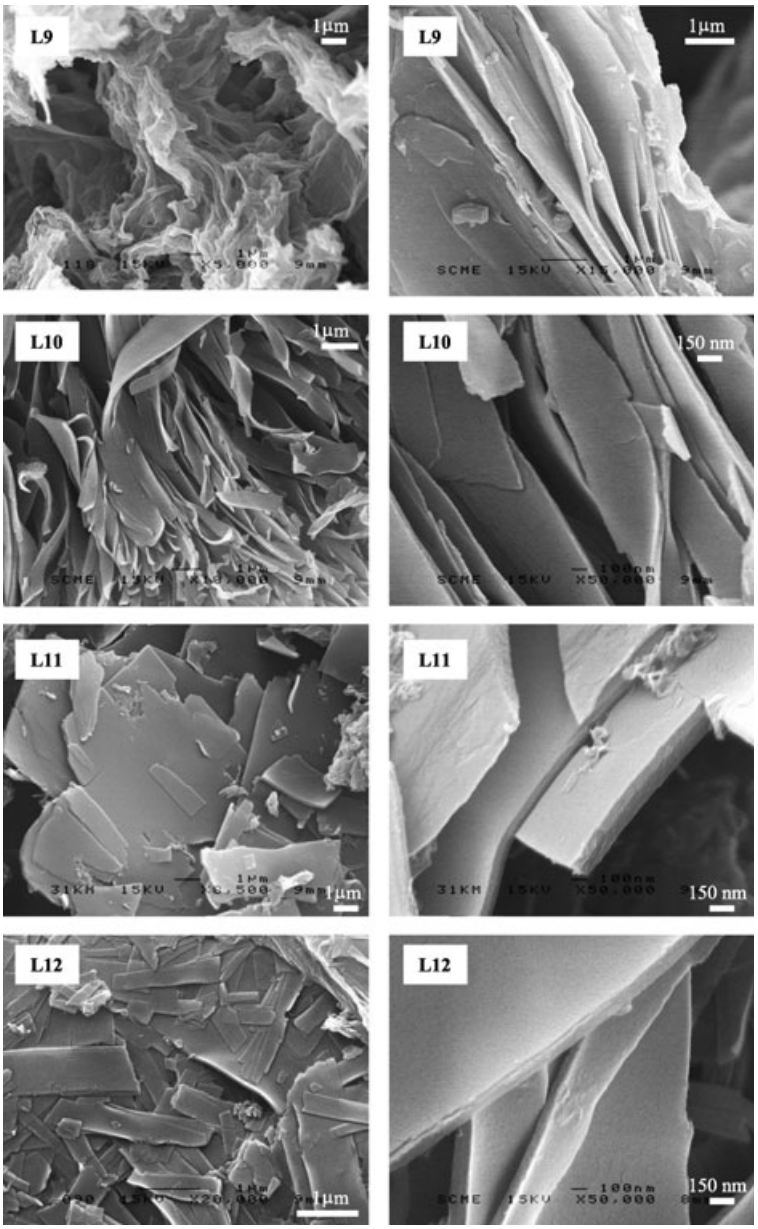

Figure 5. SEM images of ordered hybrid silicas **L9**–**L12**.

tained with the electric vector parallel to the diamond/hybrid solid interface, V-polarisation to transmission spectra with the electric vector at 45° to the interface. The amorphous hybrid **A12** gave similar H- and V-polarisation spectra. Conversely, strong polarisation dependence was observed in the case of **L12**, both for amide I ($\nu_{C=O}$) and for amide II (δ_{N-H}). The modes at 1618 cm^{-1} ($\nu_{C=O}$) and 1583 cm^{-1} (δ_{N-H}) in the H-polarisation shift to 1621 and 1579 cm^{-1}, respectively, in the V-polarisation. Similar results were obtained for materials **A10**, **A11**, **L10** and **L11**. The $\Delta\nu$ values are given in Table 1.

The strong decrease in $\Delta\nu$ in the lamellar hybrid is in perfect agreement with the presence of oriented hydrogen-bonded urea groups in the lamellar hybrids. The lower value of $\Delta\nu$ in H-polarisation in relation to that in V-polarisation is related to a more significant contribution of hydrogen-bond strength for modes polarised in the H-polarisation than in the V-polarisation. The pressure applied on the sample induces orientation of the layered hybrid parallel to the ATR prism surface. The above observations are consistent with the model in Scheme 4 with hydrogen-bonded urea groups in planes perpendicular to the lamellae and carbonyl groups oriented parallel to the lamellar plan.

Discussion: The above results show that the synthesis of the hybrid solid, the result of the formation of strong covalent siloxane (Si–O–Si) bonds, is controlled by weak intermolecular interactions between the organic substructures. This shows that self-organisation processes can be easily used in hybrid silsesquioxanes to produce nanostructured materials. The combination of hydrogen-bonding interactions and hydrophobic interactions appeared crucial in directing the hybrid network formation.

The reaction conditions also have a crucial role. A large excess of water in the hydrolysis–condensation step appeared necessary. Organised lamellar hybrids were obtained in water, whereas the use of a stoichiometric amount of water in ethanol afforded amorphous solids. This is probably related to more favourable development of hydrophobic interactions in water than in the less polar ethanol. The nature of the catalyst also plays an important role. As already mentioned,

Table 1. Polarisation dependence of $\Delta\nu$ ($= \nu_{C=O}-\delta_{N-H}$) values for **A10**–**A12** and **L10**–**L12**.

Amorphous or lamellar hybrid	$\Delta\nu$ [cm^{-1}] H-polarisation	$\Delta\nu$ [cm^{-1}] V-polarisation
A10	62	62
A11	62	62
A12	66	66
L10	34	39
L11	33	40
L12	35	42

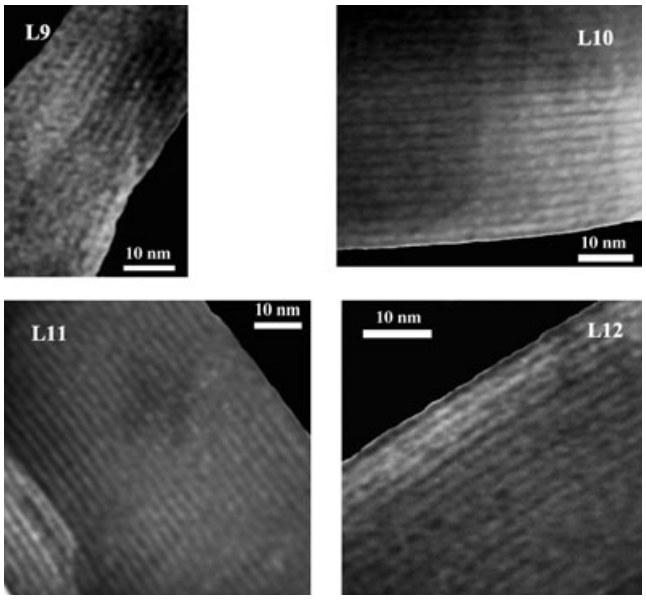

Figure 6. TEM images of lamellar hybrid silicas **L9**–**L12**.

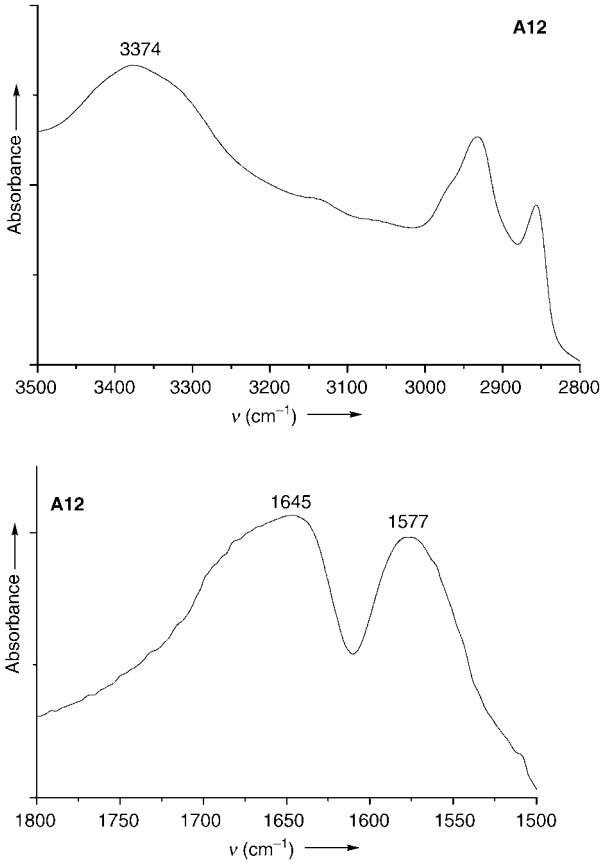

Figure 7. IR spectrum of amorphous hybrid silica **A12**.

catalysis by nucleophilic fluoride ion, which allows fast condensation, results in an amorphous material. Conversely, acid catalysis, which allows fast hydrolysis and slower condensation than under nucleophilic catalysis conditions, provides organised lamellar solids. Accordingly, the average degree of condensation of the siloxane network appeared higher for the amorphous material produced by fluoride ion-catalysed hydrolysis–condensation than for the organised material arising from acid catalysis of the reaction (90 versus 65%). Clearly, rapid condensation to form a rigid and a highly condensed siloxane network resulted in amorphous material. In contrast, the slower and more limited condensation to form a more flexible siloxane network favoured the arrangement of the organic fragments, which self-assembled through a combination of hydrogen-bonding interactions between urea groups and hydrophobic interactions between the alkylene chains. The precursors, which hydrolyse to Si–OH-containing molecules, behave as amphiphilic molecules capable of self-assembly (Scheme 5).

The production of dimeric or oligomeric association of the precursor molecules may enhance inter-aggregate condensation rates. We have previously reported entropy-favoured condensation by use of metal templating effects for related materials.[15] The condensation can produce ladder-type oligomeric structures, which may then condense into a layered network. However further studies to clarify the exact mechanistic pathway are necessary. Whereas the precursors dissolved in ethanol, they did not completely dissolve in water upon hy-

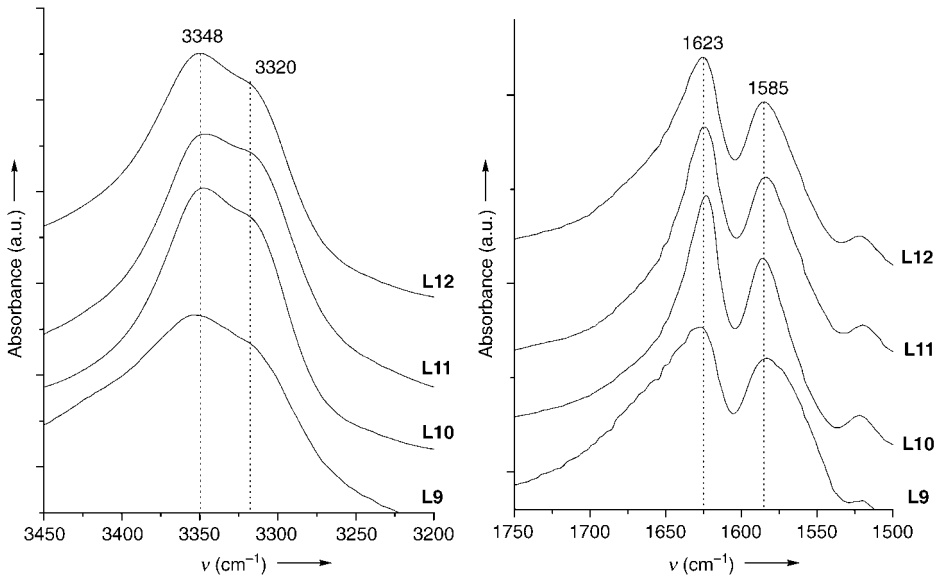

Figure 8. IR spectra of lamellar hybrid silicas **L9**–**L12**.

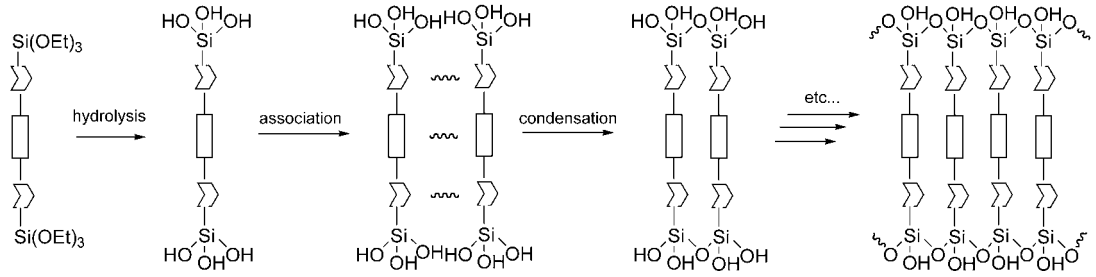

Scheme 5. Schematic representation of the hydrolysis–condensation process affording organised hybrids.

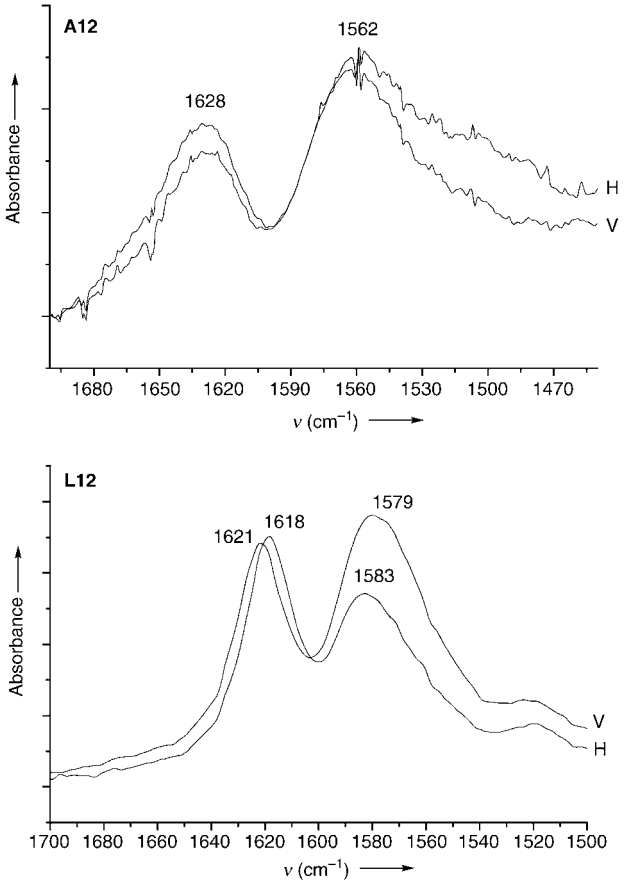

Figure 9. Polarisation dependence of the FTIR-ATR spectra of **A12** and **L12**.

drolysis of Si–OEt groups. The reaction mixture is heterogeneous and the hybrid network formation may also arise from some hydrolysis–condensation in the solid state. The use of a soluble phenylene-bridged precursor has recently allowed a better insight into the self-organisation mechanism.[20] The above studies allowed self-organised hybrids to be generated on the basis of the self-assembly properties of the molecular precursors. Hydrogen-bonding interactions between organic substructures in the hybrid network appeared stronger than intermolecular hydrogen bonding in the microcrystalline precursor. Strongly oriented hydrogen-bonded urea groups were characterised in the case of the organised lamellar solid. The role of the hydrocarbon chain is also important, since some amorphous contribution appeared in the lamellar material upon reduction of the chain length to nine carbon atoms.

Conclusion

Hybrid silsesquioxane materials are of great interest in offering a possible synthesis of nanostructured materials by design. In the context of molecular engineering, the self-condensation properties of the precursor molecules can be tuned to form supramolecular assemblies. Here a combination of hydrogen-bonding and hydrophobic interactions allowed the formation of lamellar materials, the stacking of the organic substructures directing the condensation of the inorganic silicate network. We are currently investigating the structuring of materials by supramolecular engineering. The synthesis of programmed precursor molecules with appropriate tuning of their self-assembling properties should allow the generation of materials with structuring at different nano- to microscopic scales. Moreover, the introduction of functional groups should give rise to materials of interest, for example, for molecular recognition, advanced catalysis, electronics, opto-electronics and magnetism.

Experimental Section

General information and techniques: The syntheses of the molecular precursors were carried out under nitrogen atmosphere by use of a vacuum line and Schlenk techniques. 3-Isocyanotopropyltriethoxysilane was purchased from Aldrich and was distilled before use. The other reagents and solvents were purchased from ABCR, Acros, Aldrich, Alfa-aesar, Fluka and Lancaster and were used without any further purification. *n*-Pentane was distilled from $LiAlH_4$, dichloromethane from P_2O_5, and ethanol from magnesium turnings. Melting points were determined on an electrothermal apparatus (IA9000 series) and are uncorrected. Elemental analyses were carried out by the "Service Central d'Analyse du CNRS" in Vernaison, France.

^1H, ^{13}C and ^{29}Si NMR spectra in solution were recorded on Bruker AC 200 and AC 250 spectrometers at room temperature in deuterated chloroform as solvent and with TMS as internal reference. ^1H, ^{13}C and ^{29}Si solid-state NMR spectra were obtained on Bruker FT-AM 200 or FT-AM 400 spectrometers by use of cross-polarization and magic-angle spinning techniques (CP-MAS) with TMS as reference for the chemical shifts.

BET surface areas were obtained with a Micromeritics Gemini 2375 apparatus.

TEM images were performed with a JEOL 200 CX microscope and a JEOL JEM 2010 microscope. SEM images were obtained with a JEOL 6300F apparatus.

Powder X-ray diffraction (PXRD) measurements and data treatment were performed at the "Groupe de Dynamique des Phases Condensées" in Montpellier. The X-ray diffraction experiments were carried out on solid powders in glass capillaries (1 mm diameter) in a transmission configuration. A copper rotating anode X-ray source (4 kW) with a multilayer focusing "Osmic" monochromator giving high flux (10^8 photons s^{-1}) and punctual colimation was employed. $\lambda_{K\alpha} = 1.542$ Å. An "Image plate" 2D detector was used. The diffraction curves were obtained, giving diffracted intensity as a function of the wave vector q. The diffracted intensity was corrected by exposition time, transmission and intensity background coming from diffusion by an empty capillary.

Routine IR data were obtained on a Perkin–Elmer 1000 FT-IR spectrophotometer.

Attenuated total reflection IR (FTIR-ATR) spectra with polarised light were measured on a Perkin–Elmer spectrum one with a KRS5 polariser.

General method for the preparation of the precursors: In a typical synthesis, 1,9-diaminononane (1.12 g, 7 mmol) was dissolved in dried dichloromethane (40 mL) under nitrogen in a Schlenk tube. 3-Isocyanatopropyltriethoxysilane (3.53 g, 14.3 mmol) was slowly added by syringe at room temperature. The mixture was stirred for 12 h and the solvent was removed in vacuum to give an off-white solid. This was washed three times with dried *n*-pentane and finally dried in vacuo.

1,9-Bis[(triethoxysilyl)propylureido]nonane (P9): Yield: 4.57 g, 90 %; m.p. 115–117 °C; ^{1}H NMR (200 MHz, $CDCl_3$): δ = 0.52–0.6 (m, 4H; CH_2Si), 1.15 (t, 18H; CH_3), 1.36–1.56 (m, 18H; 9×CH_2), 3.05–3.08 (m, 8H; CH_2–NH), 3.75 (q, 12H; OCH_2), 5.43–5.49 ppm (m, 4H; NH); ^{13}C NMR (200 MHz, $CDCl_3$): δ = 159.1 (CO), 58.3 (OCH_2), 42.8, 40.0 (2C; CN), 30.2, 29.2, 28.9, 26.6, 23.7 (5C; CH_2), 11.2 (CH_3), 7.6 ppm (CH_2Si); ^{29}Si NMR (250 MHz, $CDCl_3$): δ = −45 ppm; IR (KBr, pellet): $\tilde{\nu}$ = 957, 1076, 1104 (ν_{Si-O}), 1576 (δ_{N-H}), 1622 ($\nu_{C=O}$), 2855, 2934, 2976 (ν_{C-H}), 3342 cm^{-1} (ν_{N-H}); elemental analysis calcd (%) for $C_{29}H_{64}O_8N_4Si_2$: C 53.34, H 9.88, N 8.58; found: C 53.09, H 9.88, N 8.48.

1,10-Bis[(triethoxysilyl)propylureido]decane (P10): The preparation of this compound was as described for **P9**, but starting from 1,10-diaminodecane (1.03 g, 6 mmol) and γ-isocyanatopropyltriethoxysilane (3 g, 12.12 mmol). After drying under vacuum (2×10^{-2} mm Hg), **P10** was obtained as a white solid. Yield: 3.7 g, 93 %; m.p. 114–116 °C; ^{1}H NMR (200 MHz, $CDCl_3$): δ = 0.50–0.59 (m, 4H; CH_2Si), 1.14 (t, 18H; CH_3); 1.4, 1.55 (m, 20H; 10×CH_2); 3.0, 3.1 (m, 8H; CH_2–NH); 3.73 (q, 12H; OCH_2); 5.47 (2H; NH), 5.51 ppm (2H; NH); ^{13}C NMR (200 MHz, $CDCl_3$): δ = 159.13 (CO), 58.3 (OCH_2), 42.8, 40.2 (2×C–N), 30.2, 29.3, 29.2, 26.8, 23.7 (5×CH_2), 18.2 (CH_3), 7.6 ppm (Si–CH_2); ^{29}Si NMR (250 MHz, $CDCl_3$): δ = −45 ppm; IR (KBr pellet): $\tilde{\nu}$ = 958, 1079, 1104 (ν_{SiO}), 1576 (δ_{NH}), 1623 (ν_{CO}), 2853, 2932, 2976 (ν_{CH}), 3341 cm^{-1} (ν_{NH}); elemental analysis calcd (%) for $C_{30}H_{66}O_8N_4Si_2$: C 54.02, H 9.97, N 8.40; found: C 53.70, H 9.91, N 8.34.

1,12-Bis[(triethoxysilyl)propylureido]dodecane (P12): The preparation of this compound was as described for **P9**, but starting from 1,12-diaminododecane (1.6 g, 8 mmol) and γ-isocyanatopropyltriethoxysilane (4 g, 16.1 mmol). After drying under vacuum (2×10^{-2} mm Hg), **P12** was obtained as a white solid. Yield: 5.2 g, 93 %, m.p. 120–121 °C; ^{1}H NMR (200 MHz, $CDCl_3$): δ = 0.56–0.65 (m, 4H; CH_2Si), 1.19 (t, 18H; CH_3), 1.4, 1.62 (m, 24H; 12×CH_2), 3.0, 3.13 (m, 8H; CH_2–NH), 3.78 (q, 12H; OCH_2), 5.89 (2H; NH), 5.0 ppm (2H; NH); ^{13}C NMR (200 MHz, $CDCl_3$): δ = 158.7 (CO), 58.4 (OCH_2), 42.9, 40.5 (2×C–N), 30.3, 29.4, 29.3, 29.2, 26.8, 23.7 (6×CH_2), 18.3 (CH_3), 7.6 ppm (Si–CH_2); ^{29}Si NMR (250 MHz, $CDCl_3$): δ = −45.3 ppm; IR (KBr, pellet): $\tilde{\nu}$ = 958, 1079, 1168 (ν_{SiO}), 1577 (δ_{NH}), 1625 (ν_{CO}), 2851, 2930, 2976 (ν_{CH}), 3347 cm^{-1} (ν_{NH}); elemental analysis calcd (%) for $C_{32}H_{70}O_8N_4Si_2$: C 55.29, H 10.15, N 8.06; found: C 55.02, H 10.21, N, 8.26.

Undecane-1,11-dioyl dichloride: Under nitrogen, thionyl chloride (3.46 g, 29 mmol) was slowly added to a stirred solution of undecane-1,11-dicarboxylic acid (1.95 g, 8 mmol) suspended in dry CH_2Cl_2 (20 mL). After the mixture had been heated at reflux overnight, the solvent and unreacted thionyl chloride were evaporated in vacuum and the residual liquid was distilled. Yield: 2 g, 90 %; b.p. 120–122 °C (5×10^{-2} mm Hg); ^{1}H NMR (200 MHz, $CDCl_3$): δ = 1.27 (m, 14H; CH_2), 1.7 (m, 4H; CH_2CH_2CO), 2.87 ppm (t, 4H; CH_2CO); ^{13}C NMR (200 MHz, $CDCl_3$): δ = 173.73 (CO), 47.07 (CH_2CO), 29.31, 29.21, 28.99, 28.37, 25.03 (5×CH_2); IR (KBr): $\tilde{\nu}$ = 1794 cm^{-1} (ν_{CO}).

1,11-Diisocyanatoundecane: Undecane-1,11-dioyl dichloride (3.73 g, 13.3 mmol) in acetone (5 mL) was added slowly to a cooled solution (0 °C) of sodium azide (3.58 g, 55.16 mmol) in acetone (30 mL). After stirring for 4 h (0 °C to RT), the reaction mixture was transferred under nitrogen into a three-necked flask containing toluene (440 mL) and the mixture was heated at 65 °C overnight. The solvent was removed and the liquid residue was filtered on celite and washed with pentane. The solvent was removed under vacuum and the liquid residue was purified by distillation. Yield: 2.3 g, 73 %; b.p.: 114 °C (5×10^{-2} mm Hg); ^{1}H NMR (200 MHz, $CDCl_3$): δ = 1.31 (m, 14H; CH_2), 1.53–1.63 (m, 4H; CH_2CH_2CO), 3.28 ppm (t, 4H; CH_2NCO); ^{13}C NMR (200 MHz, $CDCl_3$): δ = 93.7 (NCO), 42.98 (CH_2NCO), 31.28, 29.38, 28.9, 26.5 ppm (4×CH_2); IR (KBr): $\tilde{\nu}$ = 2274 cm^{-1} (ν_{NCO}); elemental analysis calcd (%) for $C_{13}H_{22}O_2N_2$: C 65.5, H 9.31, N 11.76; found: C 65.63, H 9.39, N 11.85.

1,11-Bis[(triethoxysilyl)propylureido]undecane (P11): (3-Aminopropyl)-triethoxysilane (4.33 g, 19.58 mmol) was slowly added at 0 °C to a stirred solution of 1,11-diisocyanatoundecane (2.32 g, 9.74 mmoles) in dry CH_2Cl_2 (20 mL). After the mixture had been stirred overnight, the solvent was removed in vacuo to yield an off-white solid. Unreacted (3-aminopropyl)triethoxysilane was removed by washing with dry pentane. After drying under vacuum (2×10^{-2} mm Hg), **P11** was obtained as a white solid. Yield: 5.3 g, 80 %; m.p.: 112–114 °C; ^{1}H NMR (200 MHz, $CDCl_3$): δ = 0.57–0.65 (m, 4H; CH_2Si), 1.2 (t, 18H; CH_3), 1.44, 1.58 (m, 22H; 11×CH_2), 3.07, 3.17 (m, 8H; CH_2–NH), 3.78 (q, 12H; OCH_2), 4.87 (2H; NH), 4.98 ppm (2H; NH); ^{13}C NMR (200 MHz, $CDCl_3$): δ = 158.84 (CO), 58.37 (OCH_2), 42.85, 40.33 (2×C–N), 30.27, 29.29, 29.20, 29.14, 26.76, 23.69 (6×CH_2), 18.26 (CH_3), 7.62 ppm (Si–CH_2); ^{29}Si NMR (250 MHz, $CDCl_3$): δ = −45.1 ppm; IR (KBr, pellet): $\tilde{\nu}$ = 958, 1079, 1106 (ν_{SiO}), 1577 (δ_{NH}), 1623 (ν_{CO}), 2851, 2931, 2976 (ν_{CH}), 3346 cm^{-1} (ν_{NH}); elemental analysis calcd (%) for $C_{31}H_{68}O_8N_4Si_2$: C 54.67, H 10.07, N 8.23; found: C 54.68, H 10.03, N 8.40.

Acid-catalysed hydrolysis and polycondensation

General method for the preparation of the lamellar bridged silsesquioxanes L9–12: A mixture containing a molar ratio of **Px**/H_2O/HCl 1:600:0.2 was vigorously stirred at 80 °C for 1 h and then allowed to stand for 48 h at the same temperature. The solid, which formed quantitatively, was recovered by filtration and was successively washed with H_2O, EtOH and acetone. After drying (110 °C, 6 h) the solid was collected as a white powder.

Synthesis of L9: ^{13}C CP MAS NMR: δ = 11.6, 31.7, 43.4, 160.1 ppm; ^{29}Si CP MAS NMR: δ = −38.4, −48.7, −57.8 ppm; IR (KBr, pellet): $\tilde{\nu}$ = 917 (ν_{Si-OH}), 1030.4, 1128.2 (ν_{Si-O}), 1584 (δ_{NH}), 1629.1 (ν_{CO}), 2855.5 (ν_{CHsym}), 2931.7 (ν_{CHasym}), 3355.4 cm^{-1} (ν_{NH}); N_2 BET surface area: 13.1 m^2g^{-1}; elemental analysis calcd (%) for $C_{17}H_{36}O_6N_4Si_2$: C 45.51, H 8.09, N 12.49, Si 12.52; found: C 44.83, H 8.17, N, 12.25, Si 11.9.

Synthesis of L10: ^{13}C CP MAS NMR: δ = 11.6, 26.4, 31.5, 34.0, 42.8, 160.2 ppm; ^{29}Si CP MAS NMR: δ = −48.12, −57.02, −66.56 ppm; IR (KBr, pellet): $\tilde{\nu}$ = 892, 1022, 1095 (ν_{SiO}), 1586 (δ_{NH}), 1623 (ν_{CO}), 2851 (ν_{CHsym}), 2927 (ν_{CHasym}), 3346 cm^{-1} (ν_{NH}); N_2 BET surface area: 43.2 m^2g^{-1}; elemental analysis calcd (%) for $C_{18}H_{38}O_6N_4Si_2$: C 46.73, H 8.28, N 12.11, Si 12.14; found: C 46.88, H 8.24, N 12.12, Si 12.30.

Synthesis of L11: ^{13}C CP MAS NMR: δ = 12.2, 25.5, 33.3, 43.4, 160.3 ppm; ^{29}Si CP MAS NMR: δ = −38.9, −48.5, −57.3, −66.7 ppm; IR (KBr, pellet): $\tilde{\nu}$ = 919, 1030, 1115 (ν_{SiO}), 1585 (δ_{NH}), 1625 (ν_{CO}), 2855 (ν_{CHsym}), 2932 (ν_{CHasym}), 3348 cm^{-1} (ν_{NH}); N_2 BET surface area : 60.4 m^2g^{-1}; elemental analysis calcd (%) for $C_{19}H_{40}O_6N_4Si_2$: C 47.87, H 8.46, N 11.75, Si 11.78; found: C 47.85, H 8.48, N 12.01, Si 11.7.

Synthesis of L12: ^{13}C CP MAS NMR: δ = 11.1, 27.0, 31.5, 34.2, 42.9, 160.1 ppm; ^{29}Si CP MAS NMR: δ = −49, −58, −67 ppm; IR (KBr,

pellet): $\tilde{\nu}$ = 893, 1023, 1125 (ν_{SiO}), 1585 (δ_{NH}), 1625 (ν_{CO}), 2850 (ν_{CHsym}), 2923 (ν_{CHasym}), 3349 (ν_{NH}) cm^{-1}; N_2 BET surface area: 41.7 m^2g^{-1}; elemental analysis calcd (%) for $C_{20}H_{42}O_6N_4Si_2$: C 48.95, H 8.63, N 11.42, Si 11.45; found: C 48.51, H 8.74, N 11.49, Si 11.15.

Fluoride-catalysed hydrolysis and polycondensation

General method for the preparation of the amorphous bridged silsesquioxanes A9–12: These materials were synthesised by hydrolysis of the silylated bis-urea precursor in a mixture of ethanol, water and NH_4F at a molar ratio of **P*x***/EtOH/H_2O/NH_4F 1:60:6:0.01. The reaction was carried out as follows: **P*x*** was dissolved in freshly distilled ethanol containing NH_4F and water and the homogeneous solution was allowed to stand at 20°C. Gelation had occurred after 24 h. After curing at 20°C for 48 h, the gel was powdered. After air drying, the solid was collected, washed with EtOH and acetone and then dried (110°C, 6 h), yielding a white powder.

Synthesis of A9: ^{13}C CP MAS NMR: δ = 10.2, 18.5, 30.1, 41.1, 161 ppm; ^{29}Si CP MAS NMR: δ = −58.7, −66.3 ppm; IR (KBr, pellet): $\tilde{\nu}$ = 941.2 (ν_{Si-OH}), 1003, 1138 (ν_{SiO}), 1566.6 (δ_{NH}), 1657.1 (ν_{CO}), 2851.6 (ν_{CHsym}), 2928.2 (ν_{CHasym}), 3339.7 (ν_{NH}) cm^{-1}; N_2 BET surface area: 3.8 m^2g^{-1}; elemental analysis calcd (%) for $C_{17}H_{34}O_5N_4Si_2$: C 47.41, H 7.96, N 13.01, Si 13.04; found: C 46.60, H 8.13, N 12.41, Si 12.35.

Synthesis of A10: ^{13}C CP MAS NMR: δ = 10.3, 18.8, 30.0, 41.4, 159.9 ppm; ^{29}Si CP MAS NMR: δ = −59.0, −66 ppm; IR (KBr, pellet): $\tilde{\nu}$ = 920, 1029, 1132 (ν_{SiO}), 1572 (δ_{NH}), 1645 (ν_{CO}), 2857 (ν_{CHsym}), 2931 (ν_{CHasym}), 3380 (ν_{NH}) cm^{-1}; N_2 BET surface area: 7 m^2g^{-1}; elemental analysis calcd (%) for $C_{18}H_{36}O_5N_4Si_2$: C 48.62, H 8.16, N 12.6, Si 12.63; found: C 46.89, H 8.23, N 11.99, Si 12.0.

Synthesis of A11: ^{13}C CP MAS NMR: δ = 11.0, 18.7, 30.3, 41.1, 58.,160.2 ppm; ^{29}Si CP MAS NMR: δ = −58.5, −66.6 ppm; IR (KBr, pellet): $\tilde{\nu}$ = 917, 1026, 1131 (ν_{SiO}), 1571 (δ_{NH}), 1646 (ν_{CO}), 2858 (ν_{CHsym}), 2932 (ν_{CHasym}), 3384.8 (ν_{NH}) cm^{-1}; N_2 BET surface area: 2.2 m^2g^{-1}; elemental analysis calcd (%) for $C_{19}H_{38}O_5N_4Si_2$: C 49.75, H 8.35, N 12.21, Si 12.25; found: C 48.23, H 8.37, N 12.19, Si 11.90.

Synthesis of A12: ^{13}C CP MAS NMR: δ = 10.7, 30.4, 40.3, 159.9 ppm; ^{29}Si CP MAS NMR: δ = −58.54, −66.48 ppm; IR (KBr, pellet): $\tilde{\nu}$ = 920, 1027, 1136 (ν_{SiO}), 1574 (δ_{NH}), 1646 (ν_{CO}), 2856 (ν_{CHsym}), 2932 (ν_{CHasym}), 3374 (ν_{NH}) cm^{-1}; N_2 BET surface area: 3.5 m^2g^{-1}; elemental analysis calcd (%) for $C_{20}H_{40}O_5N_4Si_2$: C 50.82, H 8.53, N 11.85, Si 11.88; found: C 48.77, H 8.64, N 11.24, Si 11.3.

Acknowledgements

The authors gratefully acknowledge the "Ministère de la Recherche" (ACI 2000: Physicochimie de la matière complexe) and the CNRS for financial supports.

[1] a) C. Sanchez, F. Ribot, *New J. Chem.* **1994**, *18*, 1007–1047; b) *Organic/inorganic hybrid materials* (Eds.: R. M. Laine, C. Sanchez, C. J. Brinker, E. Giannelis), *MRS Symp. vol.* 519, **1998**; c) *Organic/inorganic hybrid materials II*, (Eds.: R. M. Klein, M. Deguire, F. Lorraine, J. Mark), *MRS Symp. vol*. 576, **1999**; d) *Organic/inorganic hybrid materials III* (Eds.: R. M. Laine, C. Sanchez, C. J. Brinker), *MRS Symp*. vol. 628, **2000**; e) J. J. E. Moreau, L. Vellutini, M. Wong Chi Man, C. Bied, J-L. Bantignies, P. Dieudonné, J-L. Sauvajol, *Mater. Res. Soc. Symp. Proc.* **2002**, *726*, 235–242.

[2] *Functional Hybrid Materials* (Eds.: P. Gomez-Romero, C. Sanchez), Wiley-VCH, **2004**.

[3] a) K. J. Shea, D. A. Loy, O. W. Webster, *Chem. Mater.* **1989**, *1*, 512–513; b) K. J. Shea, D. A. Loy, O. W. Webster, *J. Am. Chem. Soc.* **1992**, *114*, 6700–6710.

[4] R. J. P. Corriu, J. J. E. Moreau, P. Thépot, M. Wong Chi Man, *Chem. Mater.* **1992**, *4*, 1217–1224.

[5] a) D. A. Loy, K. J. Shea, *Chem. Rev.* **1995**, *95*, 1431–1442; b) R. J. P. Corriu, D. Leclercq, *Angew. Chem.* **1996**, *108*, 1524–1540; *Angew. Chem. Int. Ed.*, **1996**, *35*, 1420–1436; c) R. J. P. Corriu, *Angew. Chem.* **2000**, *112*, 1432–1455; *Angew. Chem. Int. Ed.* **2000**, *39*, 1376–1398; d) K. J. Shea, J. J. E. Moreau, D. Loy, R. J. P. Corriu, B. Boury, in *Functional Hybrid Materials* (Eds.: P. Gomez-Romero, C. Sanchez), Wiley-VCH, **2004**, pp. 50.

[6] a) J. J. E. Moreau, M. Wong Chi Man, *Coord. Chem. Rev.* **1998**, *178–180*, 1073–1084, and references therein; b) E. Lindner, T. Schneller, F. Auer, H. A. Mayer, *Angew. Chem.* **1999**, *111*, 2288–2309; *Angew. Chem. Int. Ed.* **1999**, *38*, 2155–2174; c) A. Adima, J. J. E. Moreau, M. Wong Chi Man, *J. Mater. Chem.* **1997**, *7*, 2331–2333; d) A. Adima, J. J. E. Moreau, M. Wong Chi Man, *Chirality* **2000**, *5–6*, 411–420; e) P. Hesemann, J. J. E. Moreau, *Tetrahedron: Asymmetry* **2000**, *11*, 2183–2194; f) U. Schubert, N. Hüsing, A. Lorenz, *Chem. Mater.* **1995**, *7*, 2010–2027.

[7] R. J. P. Corriu, J. J. E. Moreau, P. Thépot, M. Wong Chi Man, C. Chorro, J.-P. Lère-Porte, J-L. Sauvajol, *Chem. Mater.* **1994**, *6*, 640–649.

[8] a) J.-C. Broudic, O. Conocar, J. J. E. Moreau, D. Meyer, M. Wong Chi Man, *J. Mater. Chem.* **1999**, *9*, 2283–2285; b) S. Bourg, J.-C. Broudic, O. Conocar, J. J. E. Moreau, D. Meyer, M. Wong Chi Man, *J. Mater. Chem.* **2001**, *11*, 491–499; c) D. Meyer, O. Conocar, J. J. E. Moreau, M. Wong Chi Man FR 2770153, **1999**.

[9] a) E. Z. Faraggi, Y. Sorek, O. Levi, Y. Avny, D. Davidov, R. Neumann, R. Reisfield, *Adv. Mater.* **1996**, *8*, 833–835; b) F. Chaput, D. Reihl, Y. Lévy, J. P. Boilot, *Chem. Mater.* **1993**, *5*, 589–591; c) O. Dautel, J.-P. Lère-Porte, J. J. E. Moreau, M. Wong Chi Man, *Chem. Commun.* **2003**, 2662–2663; d) H. W. Oviatt, K. J. Shea, S. Kalluri, Y. Shi, W. H. Steier, L. R. Dalton, *Chem. Mater.* **1995**, *7*, 493–498; e) J. Livage, F. Babonneau, C. Sanchez, in *Sol–gel Optics: Processing and Applications* (Ed.: L. C. Klein), Kluwer, Boston, **1994**, p. 39; f) D. Avnir, S. Braun, D. Levy, M. Ottolenghi, in *Sol–gel Optics: Processing and Applications* (Ed.: L. C. Klein), Kluwer, Boston, **1994**, p. 303.

[10] R. J. P. Corriu, J. J. E. Moreau, P. Thépot, M. Wong Chi Man, *Chem. Mater.* **1996**, *8*, 100–106.

[11] a) M. E. Davis, *Nature* **2002**, *413*, 813–821; b) M. J. MacLachlan, I. Manners, G. A. Ozin, *Adv. Mater.* **2000**, *12*, 675–681.

[12] a) C. T. Kresge, M. E. Leonowicz, W. J. Roth, J. C. Vartuli, J. S. Beck, *Nature* **1992**, *359*, 710–712; b) J. S. Beck, J. C. Vartuli, W. J. Roth, M. E. Leonowicz, C. T. Kresge, K. D. Schmitt, C. T.-W. Chu, D. H. Olson, E. W. Sheppard, S. B. McCullen, J. B. Higgins, J. L. Schlenker, *J. Am. Chem. Soc.* **1992**, *114*, 10834–10843; c) S. Inagaki, Y. Fukushima, K. Kuroda, *J. Chem. Soc. Chem. Commun.* **1993**, 680–681; d) Q. Huo, D. I. Margolese, U. Ciesla, P. Feng, T. E. Gier, P. Sieger, R. Leon, P. M. Petroff, F. Schüth, G. D. Stucky, *Nature* **1994**, *368*, 317–321.

[13] a) S. Inagaki, S. Guan, Y. Fukushima, T. Ohsuna, O. Terasaki, *J. Am. Chem. Soc.* **1999**, *121*, 9611–9622; b) S. Guan, S. Inagaki, T. Ohsuna, O. Terasaki, *J. Am. Chem. Soc.* **2000**, *122*, 5660–5661; c) B. J. Melde, B. T. Holland, C. F. Blanford, A. Stein, *Chem. Mater.* **1999**, *11*, 3302–3308; d) T. Asefa, M. J. MacLachlan, N. Coombs, G. A. Ozin, *Nature* **1999**, *402*, 867–871; e) C. Yoshina-Ishii, T. Asefa, M. J. MacLachlan, N. Coombs, G. A. Ozin, *Chem. Commun.* **1999**, 2539–2540; f) M. J. MacLachlan, T. Asefa, G. A. Ozin, *Chem. Eur. J.* **2000**, *6*, 2507–2511; g) T. Asefa, C. Yoshina-Ishii, M. J. MacLachlan, G. A. Ozin, *J. Mater. Chem.* **2000**, *10*, 1751–1755; h) A. Sayari, S. Hamoudi, Y. Yang, I. L. Moudrakovski, J. R. Ripmeester, *Chem. Mater.* **2000**, *12*, 3857–3863; i) A. Stein, B. T. Melde, R. C. Schroden, *Adv. Mater.* **2000**, *12*, 1403–1419; j) Y. Lu, H. Fan, N. Doke, D. A. Loy, R. A. Assink, D. A. LaVan, C. J. Brinker, *J. Am. Chem. Soc.* **2000**, *122*, 5258–5261.

[14] a) A. Sayari, S. Hamoudi, *Chem. Mater.* **2001**, *13*, 3151–3168; b) M. P. Kapoor, Q. Yang, S. Inagaki, *J. Am. Chem. Soc.* **2002**, *124*, 15176–15177.

[15] R. J. P. Corriu, J. J. E. Moreau, P. Thépot, M. Wong Chi Man, *J. Mater. Chem.* **1994**, *4*, 987–989.

[16] A. Shimojima, K. Sugahara, K. Kuroda, *Angew. Chem.* **2003**, *115*, 4191–4194; *Angew. Chem. Int. Ed.* **2003**, *42*, 4057–4060.

[17] a) B. Boury, R. J. P. Corriu, V. Le Strat, P. Delord, M. Nobili, *Angew. Chem.* **1999**, *111*, 3366–3370; *Angew. Chem. Int. Ed.* **1999**, *38*, 3172–3173; b) F. Ben, B. Boury, R. J. P. Corriu, P. Delord, M. Nobili, *Chem. Mater.* **2002**, *14*, 730–738.

[18] S. Inagaki, S. Guan, T. Ohsuna, O. Terasaki, *Nature* **2002**, *416*, 304–307.

[19] a) J. J. E. Moreau, L. Vellutini, M. Wong Chi Man, C. Bied, *J. Am. Chem. Soc.* **2001**, *123*, 1509–1510; b) J. J. E. Moreau, L. Vellutini, M. Wong Chi Man, C. Bied, J.-L. Bantignies, P. Dieudonné, J.-L. Sauvajol, *J. Am. Chem. Soc.* **2001**, *123*, 7957–7958; c) N. Liu, K. Yu, B. Smarsly, D. R. Dunphy, Y.-B. Jiang, C. J. Brinker, *J. Am. Chem. Soc.* **2002**, *124*, 14540–14541; d) J. J. E. Moreau, L. Vellutini, M. Wong Chi Man, C. Bied, *Chem. Eur. J.* **2003**, *9*, 1594–1999.

[20] J. J. E. Moreau, B. P. Pichon, M. Wong Chi Man, C. Bied, H. Pritzkow, J.-L. Bantignies, P. Dieudonné, J.-L. Sauvajol, *Angew. Chem.* **2004**, *116*, 205–208; *Angew. Chem. Int. Ed.* **2004**, *43*, 203–206.

[21] a) Y. Ono, K. Nakashima, M. Sano, J. Hojo, S. Shinkai, *Chem. Lett.* **1999**, 1119–1120; b) J. H. Jung, Y. Ono, K. Hanabusa, S. Shinkai, *J. Am. Chem. Soc.* **2000**, *122*, 5008–5009.

[22] a) M. de Loos, J. van Esch, I. Stokroos, R. M. Kellogg, B. L. Feringa, *J. Am. Chem. Soc.* **1997**, *119*, 12675–12676; b) J. van Esch, F. Schoonbeek, M. de Loos, H. Kooijman, A. L. Spek, R. M. Kellogg, B. L. Feringa, *Chem. Eur. J.* **1999**, *5*, 937–950; c) M. de Loos, J. van Esch, R. M. Kellogg, B. L. Feringa, *Angew. Chem.* **2001**, *113*, 633–636; *Angew. Chem. Int. Ed.* **2001**, *40*, 613–616; d) V. D. Laan, B. L. Feringa, R. M. Kellogg, J. Van Esch, *Langmuir* **2002**, *18*, 7136–7140.

[23] a) J. H. Jung, Y. Ono, S. Shinkai, *Chem. Eur. J.* **2000**, *6*, 4552–4557; b) K. J. C. Van Bommel, A. Friggeri, S. Shinkai, *Angew. Chem.* **2003**, *115*, 1010–1030; *Angew. Chem. Int. Ed.* **2003**, *42*, 980–999.

[24] a) F. Lortie, S. Boileau, L. Bouteiller, *Chem. Eur. J.* **2003**, *9*, 3008–3014; b) V. Simic, L. Bouteiller, M. Jalabert, *J. Am. Chem. Soc.* **2003**, *125*, 13148–13154.

[25] J. Jadzyn, M. Stockhauser, B. Zywucki, *J. Phys. Chem.* **1987**, *91*, 754–757.

[26] *Sol–gel Science: The Physics and Chemistry of Sol–gel Processing* (Eds.: C. J. Brinker, G. W. Scherer) Acad. Press, New York, **1990**, pp. 116–136.

[27] P. Dieudonné, L. Vellutini, M. Wong Chi Man, J.-L. Bantignies, J.-L. Sauvajol, C. Bied, J. J. E. Moreau, unpublished results..

Received: October 6, 2004
Published online: January 20, 2005

